Jour. Korean Inst. Mining Geol.
Vol. 22, No. 4, p. 303-314, 1989

Gold–Silver Mineralization of the Geojae Area

Choi, Seon–Gyu*, Chi, Se–Jung, Yun, Seong–Taek***, Koh, Yong–Kwon***, and Yu, Jae–Shin****

ABSTRACT : The electrum–silver–sulfide mineralization of the Geojae island area was deposited in three stages(I, II, and carbonate) of quartz and calcite veins that crosscut Late Cretaceous volcanic rocks and granodiorite(83 m.y.). Stages I and II were terminated by the onset of fracturing and brecciation events. Fluid inclusion data suggest that the gold–sulfide–bearing stages I and II each evolved from an initial high temperature(near 370℃) to a later low temperature(near 200℃). Each of those stages represented a separate mineralizing system which cooled prior to the onset of the next stage. The relationship between homogenization temperature and salinity in stages I and II suggests a complex history of boiling, cooling and dilution. Evidence of boiling indicates a pressure of <100 bars, corresponding to a depth of 500 to 1,250m assuming lithostatic and hydrostatic pressure regimes, respectively.

Fluid inclusion and mineralogical evidence suggest that the electrum–silver mineralization was deposited at a temperature of 220–260℃ from ore fluids with salinities between 1.9 and 8.1 equivalent wt.% NaCl. Total sulfur concentration is estimated to be 10^{-3} to 10^{-4} molal. The estimated fs_2 and fo_2 range from $10^{-11.8}$ to 10^{-14} atm and 10^{-35} to 10^{-36} atm, respectively. The chemical conditions indicate that the dominant sulfur species in the ore forming fluids was a reduced form(H_2S). Rapid cooling and dilution of ore–forming fluids by mixing with less–evolved meteoric waters led to gold–silver deposition through the breakdown of the bisulfide complex($Au(HS)_2^-$) as the activity of H_2S decreased.

INTRODUCTION

Most Au–Ag vein deposits in Korea are associated with either Jurassic or Cretaceous granites(Shimazaki et at., 1981 ; Shelton et al., 1988 ; So et al., 1987 a, b, and 1988 ; So and Shelton, 1987 b). Two main types of deposit have been previously documented, each displaying consistent relationships between depth, water–to–rock ratio(degree of meteoric water involvement) and Au/Ag ratio(Shelton et al., 1988) : these are Korean–type gold deposit (Tsuchida, 1944) and more silver–rich, epithermal deposits.

Korean–type deposits, of Late Jurassic to Early Cretaceous age, are characterized by high Au /Ag ratios(1 : 3 to 2 : 1)(Shikazono and Shimizu, 1986 ; Sugaki et al., 1986). Gold deposition occurred at temperatures near 270℃ in response to boiling and cooling at depths of about 1.25km(So et al., 1987 a, 1988 ; So and Shelton 1987 b ; Shelton et al., 1988). The more silver –rich epithermal deposits, of Late Cretaceous to Tertiary age, are characterized by lower Au/Ag ratios(1 : 10 to 1 : 200). Gold–silver deposition occurred at temperatures <240℃ in response to boiling at depths of <0.75km(Park, 1983 ; So et al., 1987 a and b).

In the Geojae island area, a number of Au –Ag–Cu–Pb–Zn–Te mineralized quartz veins cut the volcanic and granitic rocks. Myeongjin and Bulgok mines are each located on such veins. The average ore grade at Myeongjin mine is 3.49g/ton of gold, 3,623g/ton of silver, 5.49wt.% lead, 13.2wt.% zinc, and 0.6wt.% copper. In this paper we document the physical and chemical conditions of ore deposition in the Geojae area.

GEOLOGY AND ORE DEPOSITS

Geology of the area consists of the Cretaceous Seongpori Formation and variety of later igneous rocks(Fig.1, Won et al., 1980). The Seongpori Formation consists of black and greenish gray shale, light gray to brown sandstone and conglomerate. In the lower part of the formation, shale beds alternate with sandstone and with a discontinuous thin conglomerate bed. Lenticular limestone beds(less than 25cm in thickness) are intercalated in shale beds. The black to dark gray upper layers of the formation display only weak bedding and consist mainly of pelitic hornfels interlayered with metasubgreywacke, metaarkosic sandstone, conglomeratic hornfels and tuffaceous hornfels.

Volcanic rocks, both intruding and overlying the Seongpori Formation, comprise andesite and andesite breccias. Andesite breccia, displaying

The research for this paper was financially supported by 1988 program of Korea Research Foundation.

* Department of Earth Science, Korea National University of Education. 363–890, Republic of Korea.
** Korea Institute of Energy and Resources, Daejeon, 301–343, Republic of Korea.
*** Department of Geology, Korea University, Seoul, 136–701, Republic of Korea.

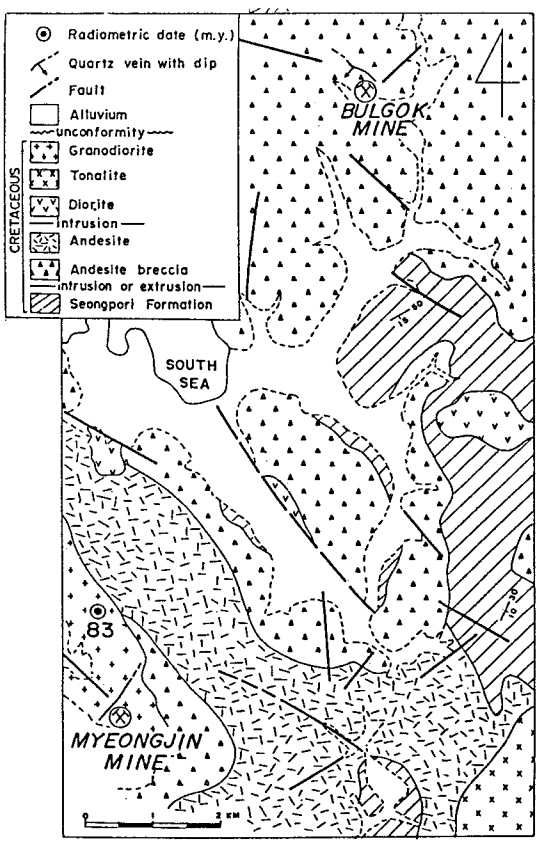

Fig. 1. Geologic map of the Geojae Au–Ag mining area. Radiometric age of the host rock (granodiorite) is shown.

flow-banding, is interlayered with discontinuous thin black shale beds and tuffaceous beds. They are dominantly autoclastic breccias, with clasts less than 30cm in size, and, more rarely, subangular alloclastic breccias containing clasts of hornfels, quartzite and diorite. The matrix is composed of plagioclase, chlorite, epidote, magnetite and rare sphene, quartz and hornblende. Andesites in gradational contact with the breccias and with each other are divided into compact andesite, porphyritic andesite, andesite porphyry and dacitic porphyritic andesite, andesite porphyry and dacitic porphyry. In their contact zones with later igneous intrusions, uralitization to pyroxene took place during contact metamorphism.

Fine to medium-grained diorite occurs mainly as small stocks. In these diorites deuteric hornblende, occurring as lath and acicular forms, is interstitial to plagioclase(oligoclase to andesine). Pyroxene often displays corona textures.

Granitic intrusions belonging to the Late Cretaceous Bulgugsa Granitic Series, vary in composition from granodiorite to tonalite.

The upper layers of the Seongpori Formation were strongly altered to various types of hornfels. Granodiorite, occurring in stocks, locally grades into hornblende granite, porphyritic and micrographic biotite granite, and, rarely, quartz monzonite. Quartz often occurs as myrmekitic or micrographic intergrowths with feldspars. A whole-rock/mineral(biotite) Rb/Sr isochron obtained for the granodiorite indicates a minimum age of 83±2.3 m.y.(Table 1).

Tonalite displays a characteristic equigranular texture and is almost homogeneous, this texture differentiating it from the granodiorite. The rock locally grades into mainly hornblende -biotite granite, fine-grained leucocratic granite and aplite along the marginal part. Quartz is intimately intergrown with orthoclase, plagioclase commonly shows compositional zoning and pyroxene has been altered mainly to hornblende and more rarely to biotite along the rims.

The gold-silver-bearing hydrothermal quartz veins of Myeongjin and Bulgok mines infill narrow fractures. The main productive vein from Myeongjin mine extends 0.5km along strike(N40°E)and its thickness varies from 0.1 to 0.5m. The main ore vein at Bulgok mine has a maximum thickness of 0.6m continues for more than 100m along strike(N60°W),and dips 75° to 80° SW. All the gold-bearing quartz veins in the mining area have a similar mineralogy and paragenesis. The gangue minerals are mainly quartz, calcite and dolomite. The ore minerals predominantly comprise base metal sulfides, rare gold, silver telluride, Pb-Bi sulfosalts and native bismuth.

Table 1. Rb-Sr Data(two-point isochrons) of Specimens from the Geojae Au-Ag Mining Area(see Fig. 1 for localities).

Sample no.	Description	^{86}Sr(ppm)	^{87}Rb(ppm)	$^{87}Sr/^{86}Sr$	$^{87}Rb/^{86}Sr$	Isochron parameters: Slope	Intercept	Date(m.y.±1σ)
G-2	Granodiorite							
	whole-rock	39.03	16.0	0.7066	0.404	1.184±0.04	0.7061±0.0009	83.3±2.3
	biotite	2.321	113.6	0.7637	48.3			

In most of the wall-rocks, hydrothermal alteration does not extend more than a few centimeters into the wall rock. Away from the vein contact, the wall-rock is altered by silicification, sericitization and chloritization. Chloritization is pervasive, usually obliterating all phenocrysts except quartz.

MINERALOGY AND PARAGENESIS

The three major stages of mineralization in the vein forming process are recognized, (I) the stage of the Au-Ag mineralization with deposition of gray quartz ; (II) repeated fracturing and deposition of milky barren quartz with rare sulfides:and(III) deposition of carbonates(Fig. 2). Each mineralization stage displays significant difference from one another with respect to microscopic mineral associations and textures.

Stage I : Economic quantities of Au and Ag, together with variable amounts of Cu, Zn, Pb, Bi, Te, and Sb were introduced during this mineralization stage. The ore vein consists mainly of gray quartz with pyrite, sphalerite, chalcopyrite, galena, tetrahedrite, marcasite, electrum, stuezite, lillianite, galenobismutite and native bismuth. The gray quartz has a superficially massive appearence but on close examination can be seen to be fine-grained along the margins of the vein and increasingly coarsely crystalline toward the center. It occasionally occurs as chalcedonic quartz at the contact with wall-rock. The ore mineralization occurs near the margin of the vein. Either as massive irregular aggregates or as disseminations interstitial to quartz occurs. The mineral paragenesis of stage I mineralization can be divided into three substages : 1) early Cu+Pb+Zn sulfides, 2) main Au-Ag telluride, and 3) late Pb-Bi sulfosalts+native bismuth.

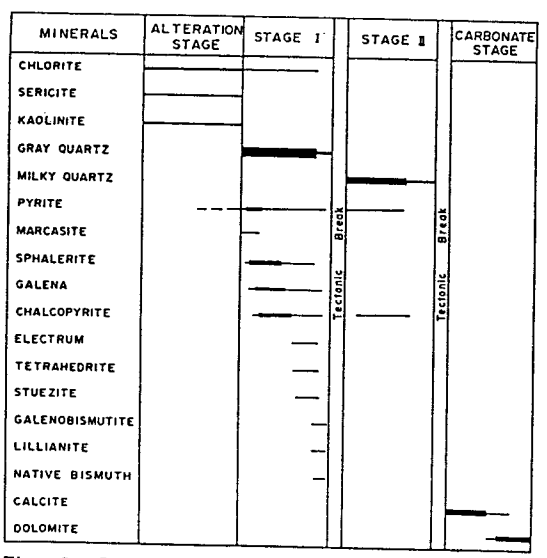

Fig. 2. Generalized paragenetic sequence of vein minerals in the Geojae Au-Ag mining area. Width of lines corresponds to relative abundance.

The early Cu+Pb+Zn sulfide substage is characterized by dominant pyrite, sphalerite, chalcopyrite, variable amounts of galena and rare marcasite. Ubiquitous pyrite is the major sulfide occurring as well-developed single crystals, crystal clusters and fine-grained disseminates. Marcasite occurs rarely as inclusions in early pyrite. Yellowish brown sphalerite is the most abundant ore mineral after pyrite and contains microscopic chalcopyrite blebs. The mole percentages of the FeS, MnS, and CdS in sphalerite by EPMA analysis are 0.15 to 1.1, 0.15 to 0.20 and 0.53 to 1.3, respectively. Chalcopyrite, in the marginal to intermediate part of the vein, is closely intergrown with sphalerite either as inclusions or as simple composite of monomineralic sulfide grains. Its grain size is comparable to that of sphalerite. Thin veinlets of chalcopyrite cross-cut sphalerite grains. Some grains contain commonly sphalerite stars. Galena normally occurs as fine-grained polymineralic aggregates associated with chalcopyrite. Thin galena veinlets often cut the sphalerite along irregular fractures and cleavages.

The main Au-Ag telluride substage is represented by tetrahedrite, electrum and stuezite(Fig. 3). Pale greenish gray tetrahedrite occurs as anhedral irregular masses(less than 200 μm in size) in the margins of the galena aggregates interstitial to the quartz matrix. Electrum(0.58 to 0.69 Ag atomic fraction), occurring as fine-grained irregular inclusions(less than 5 μm in size), is coprecipitated with stuezite in a galena matrix. Stuezite occurs as mainly rounded and rarely prismatic subhedral crystals(less than 20 μm in size) and often overgrows on small sphalerite grains in galena. Dark brown sphalerite associated with electrum and tetrahedrite in galena contains 3.8 to 5.8 mole % FeS, 0.20 to 0.28 mole % CdS and 0.23 to 0.45 mole % MnS.

The late Pb-Bi sulfosalts+native bismuth substage consists of galenobismutite, lillianite and native bismuth. Galenobismutite exsolved with galena as fine-grained, commonly disseminated, irregular grains less than 200 μm in size. These grains are often intimately intergrown with lillianite the latter rarely occurring as fine-grained anhedral crystals. Native bismuth is in the form of tiny isolated grains and is occasionally dis-

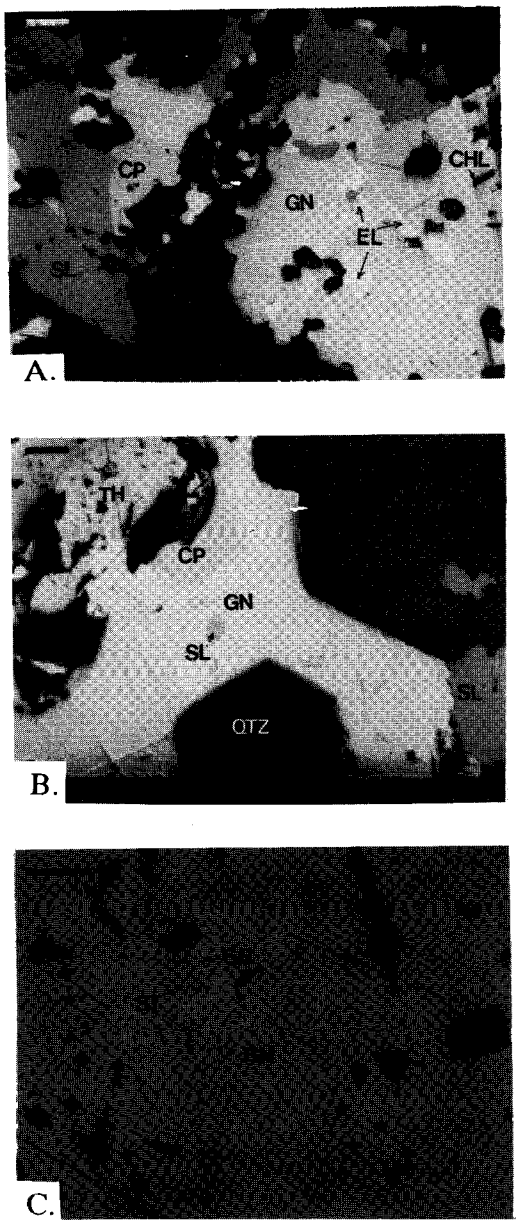

Fig. 3. Photomicrographs of ore mineral association of stage I mineralization(Myeongjin mine). Scale bars are each 0.1mm. A. Galena associated with electrum, chalcopyrite and chlorite replacing sphalerite. B. Galena replacing tetrahedrite and sphalerite, leaving unreplaced residual islands of sphalerite. C. Stuezite and galenobismutite exsolved in galena. Abbreviations : CP = chalcopyrite, CHL = chlorite, EL = electrum, GB = galenobismutite, GN = galena, QTZ = quartz, SL = sphalerite, ST = stuezite, TH = tetrahedrite.

seminated in late galena.

Stage II : The mineralization of this stage consists predominantly of milky quartz with rare pyrite and chalcopyrite. It occurs in vein containing breccias of earlier materials and many small druses comprising elongated cavities with clear quartz euhedra. Thin veinlets of comb quartz of stage II penetrated both stage I veins and their wall rocks along irregular fractures. Minor amounts of pyrite and chalcopyrite are disseminated as fine-grained euhedral to anhedral grains through the vein.

Carbonate Stage : During the latest mineralization stage, calcite and dolomite were precipitated. These carbonate veins, which are developed within pre-existing veins, do not contain ore minerals but enclose breccias of stage I ore minerals and gray quartz. Early, white, massive, fine-grained calcite deposited at both margins of the carbonate veins becomes increasingly coarsely crystalline toward their centers. Coarse-grained euhedral dolomite is precipitated on the latest calcite crystals in central portion of the vein.

FLUID INCLUSION STUDY

Fluid inclusions were examined in minerals from all the stages of mineralization in the Myeongjin and Bulgok deposits. The minerals studied were gray and milky quartz, sphalerite and calcite. Fluid inclusions were examined in thin(1mm or less) doubly polished plates. Microthermometric measurements were made using a Chaixmeca heating-freezing stage(Poty et al., 1976). Replicate measurements of homogenization temperatures showed a reproducibility within ± 2.0℃ at temperatures near 350℃. Replicate measurements of melting temperatures of H_2O and CO_2-rich standard fluid inclusions showed a reproducibility within point depression in the system H_2O-NaCl(Potter et al.,1978). The results of heating and freezing studies on fluid inclusions are presented in Table 2 and in Figures 4, 5 and 6. Three types of inclusion were recognized on the basis of their phase relations at the room temperature.

Type I fluid inclusions(liquid-rich) contain a liquid and a small vapor bubble comprising between 10 and 30 percent of the total volume of each inclusion at room temperature. The bubbles are considered to be essentially H_2O vapor because there is no indications of high CO_2 contents such as would be revealed by the formations of liquid CO_2 below 31℃ or CO_2 hydrates at temperatures near 0℃. This is the predominant type of inclusion in the samples studied and they homogenized to the liquid phase.

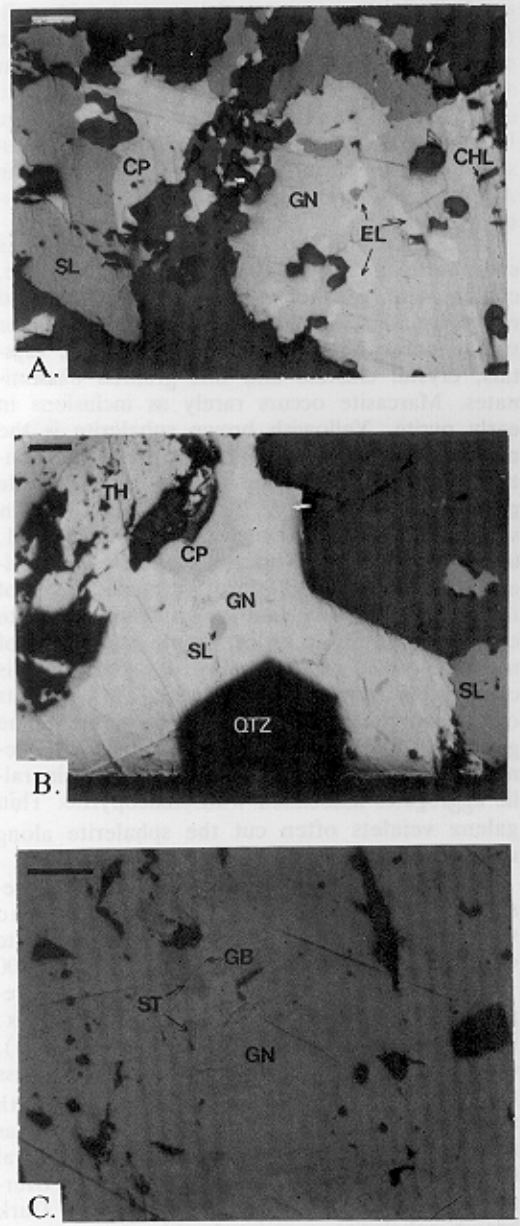
CP
CHL
GN
EL
SL
A.
TH
CP
GN
SL
SL
QTZ
B.
GB
ST
GN
C.

Table 2. Mineralogy, Parageneses, and Fluid Inclusion Data for Samples of the Geojae Au-Ag Mining Area.

Sample No.	Stage	Vein mineralogy	Inclusion in mineral	Inclusion type		Primary inclusions			Secondary inclusions	
				P	S	T_h(℃)	T_m(℃)	% NaCl*	T_h(℃)	% NaCl*
MYEONGJIN MINE										
MJI-83	I	gr qtz+py+sl+cpy +gn+tet	gr qtz	I(14)	I(2)	278 to 365			138 to 183	
MJI-35	I	gr+qtz+py+sl+cpy +gn+tet+el+stu	gr qtz	I(42)	I(12)	244 to 327	-3.4 to -5.2	5.5 to 8.1	127 to 217	4.6 to 6.6
				II(7)		311 to 324				
MJI-54	I	gr qtz+py+sl+cpy +gn	gr qtz	I(31)		284 to 350				
MJI-64	I	gr qtz+py+sl+cpy +gn	gr qtz	I(19)		252 to 333				
MJI-31	I	gr qtz+py+sl+cpy +gn+gb+Bi	gr qtz	I(26)	I(3)	245 to 295	-2.4 to -3.1	4.0 to 5.1	222 to 240	
MJI-74	I	gr qtz+py+sl+cpy +gn	gr qtz	I(28)	I(1)	280 to 370	-1.7 to -3.6	2.9 to 5.8	221	
				II(13)		312 to 321				
MJI-79	I	gr qtz+py+sl+cpy +gn	gr qtz	I(14)	I(2)	304 to 350			211 to 244	
MJI-17	I	gr qtz+py+sl+cpy +gn+tet+el	gr qtz	I(18)	I(4)	250 to 321			121 to 227	
MJI-27	I	gr qtz+py+sl+cpy +gn+gb+lil+Bi	gr qtz	I(9)	I(2)	255 to 275			159 to 182	
MJI-12	I	gr qtz+py+sl+cpy +gn	gr qtz	I(31)	I(3)	254 to 346			179 to 201	
MJI-21	I	gr qtz+py+sl+cpy +gn+tet+el+stu	gr qtz	I(32)	I(6)	246 to 300	-1.7 to -2.9	2.9 to 4.8	146 to 212	
MJI-23	I	gr qtz+py+sl+cpy +gn	gr qtz	I(19)	I(4)	264 to 347			167 to 232	
MJI-25	I	gr qtz+py+sl+el+stu	gr qtz	I(24)	I(4)	256 to 342			157 to 221	
MJI-42	I	gr qtz+py+sl+cpy +gn+tet	gr qtz	I(10)	I(7)	287 to 331			169 to 226	
MJI-46	I	gr qtz+py+sl+cpy +gn	gr qtz	I(27)	I(3)	282 to 339			171 to 196	
MJI-28	I	gr qtz+py+sl+cpy +gn	sl	I(9)		289 to 318	-4.8 to -5.2	7.6 to 8.1		
MJI-29	I	gr qtz+py+sl+cpy +gn	sl	I(6)		292 to 318				
MJII-92	II	milky qtz+py	milky qtz	I(9)	I(10)	298 to 347			142 to 209	
MJII-21	II	milky qtz	milky qtz	I(14)	I(1)	257 to 312			181	
				II(2)		302 to 307				
MJII-96	II	milky qtz	milky qtz	I(11)	I(1)	271 to 355			171	
MJII-34	II	milky qtz	milky qtz	I(18)		271 to 344				
				II(3)		301 to 309				
MJII-95	II	milky qtz	milky qtz	I(12)	I(6)	262 to 344	-1.3 to -1.9	2.2 to 3.2	127 to 192	
MJII-58	II	milky qtz	milky qtz	I(12)	I(6)	262 to 309			156 to 218	
MJII-19	II	milky qtz+py+cpy	milky qtz	I(8)	I(3)	249 to 350			172 to 207	
MJII-42	II	milky qtz	milky qtz	I(32)	I(4)	236 to 343	-1.1 to -1.4	1.9 to 2.4	146 to 203	
MJII-43	II	milky qtz	milky qtz	I(9)	I(3)	262 to 332			151 to 214	
MJII-46	II	milky qtz	milky qtz	I(21)	I(5)	243 to 337	-1.5 to -1.9	2.6 to 3.2	162 to 207	
MJII-48	II	milky qtz	milky qtz	I(22)	I(7)	241 to 329			156 to 183	
BULGOK MINE										
BGI-57	I	gr qtz+py+sl+cpy +gn+el	gr qtz	I(6)	I(4)	262 to 360			198 to 214	

Table 2. continued

BGI-51	I	gr qtz+py+sl+cpy +gn+cpy+el	gr qtz	I(24) I(4)	244 to 350			166 to 197
BGI-7	I	gr qtz+py+sl+cpy +gn+gb+lil	gr qtz	I(12)	229 to 327			
BGI-16	I	gr qtz+py+sl+cpy +gn	gr qtz	I(8) I(6)	271 to 342			131 to 207
BGI-9	I	gr qtz+py+sl+cpy +gn	gr qtz	I(15) I(4)	269 to 342			137 to 157
BGI-109	I	gr qtz	gr qtz	I(16) I(8)	297 to 350			162 to 217
BGI-6	I	gr qtz+py	gr qtz	I(10) I(2)	259 to 291	-1.9 to -2.1	3.2 to 3.6	198 to 212
BGI-18	I	gr qtz	gr qtz	I(13) I(5)	292 to 337			152 to 188
BGI-25	I	gr qtz	gr qtz	I(46) I(8)	223 to 352	-2.6 to -3.0	4.3 to 4.9	151 to 182
BGI-28	I	gr qtz	gr qtz	I(20) I(3)	238 to 332			136 to 208
BGI-22	I	gr qtz	gr qtz	I(24) I(5)	231 to 358			164 to 192
BG101	III	calcite	calcite	I(13)	207 to 246			

Abbreviations : qtz=quartz, py=pyrite, sl=sphalerite, cpy=chalcopyrite, gn=galena, tet=tetrahedrite, el=electrum, stu=stuezite, Bi=native bismuth, gb=galenobismutite, lil=lillianite, gr=gray, P=primary inclusion, S=secondary inclusion. * reported as equiv. wt. %.

These inclusions rarely contain isotrophic and cubic daughter minerals and are found in quartz and sphalerite.

Type II fluid inclusions (vapor-rich) contain liquid plus a large vapor bubble comprising more than 60 volume percent at room temperature. These inclusions homogenize to the vapor phase. This type of inclusion is found only in stage I and II quartz. Vapor-rich inclusions do not contain daughter minerals.

Inclusions in Stage I Minerals

The stage I minerals examined were gray quartz and sphalerite. Gray quartz contains numerous liquid-rich inclusions but only rare vapor-rich inclusions. The inclusions vary in size from 5 to 40 microns. The homogenization temperatures of primary type I inclusions in stage I gray quartz of the Myeongjin and Bulgok mines ranges from 244 to 370℃(311 to 324℃ for type II inclusion) and 223 to 360℃, respectively. Most sphalerites are too opaque for fluid inclusion studies, but two samples of sphalerite from stage I from Myeongjin mine had usable type I inclusions and yielded homogenization temperatures between 289 and 318℃(Fig. 4). The salinities of primary type I fluid inclusions in stage I gray quartz from the Myeongjin and Bulgok mines range from 2.9 to 8.1 and 3.2 to 4.9 equivalent weight percent NaCl, respectively. The salinities of primary type I fluid inclusion of sphalerite from Myeongjin mine range from 7.6 to 8.1 equivalent weight percent NaCl(Fig. 5).

Inclusions in Stage II Minerals

The only stage II mineral examined was milky quartz which contains primary and secondary type I and II inclusions. Type I is the most common and primary type I inclusions have a small cavity volume of 5~20 microns in diameter. The less common type II inclusions are between 20 and 40 microns in diameter. The homogenization temperature of primary type I inclusions in stage II milky quartz from Myeongjin Mine range from 236 to 355℃ as compared to 301 to 309℃ for type II inclusion (Fig. 4).

The salinities of primary type I inclusions in milky quartz from the Myeongjin Mine range from 1.9 to 3.2 equivalent weight percent NaCl (Fig. 5).

Inclusions in Carbonate Stage Minerals

Rhombohedral calcite from carbonate stage veins contains only liquid-rich type I fluid inclusions. Primary type I inclusions are 20 to 50 microns in diameter and occur in small planar groups. Rhombohedral calcite yields fluid inclusion homogenization temperatures in the range from 207 to 246℃(Fig. 4).

Variation of Hydrothermal Fluid Temperatures and Compositions

Fluid inclusion data indicate that stage I and II evolved from initial high temperatures(near 370℃). Each stage represents a separate mineralizing system which largely abated prior to the onset of the next.

The relationship between homogenization temperature and salinity in stage I(Fig. 6) suggests a complex history of boiling, cooling and dilution. During the early portion of stage I, boiling led to increase in salinity. Later cooling and dilution of ore fluids by mixing with less-evolved meteoric waters resulted in the linear

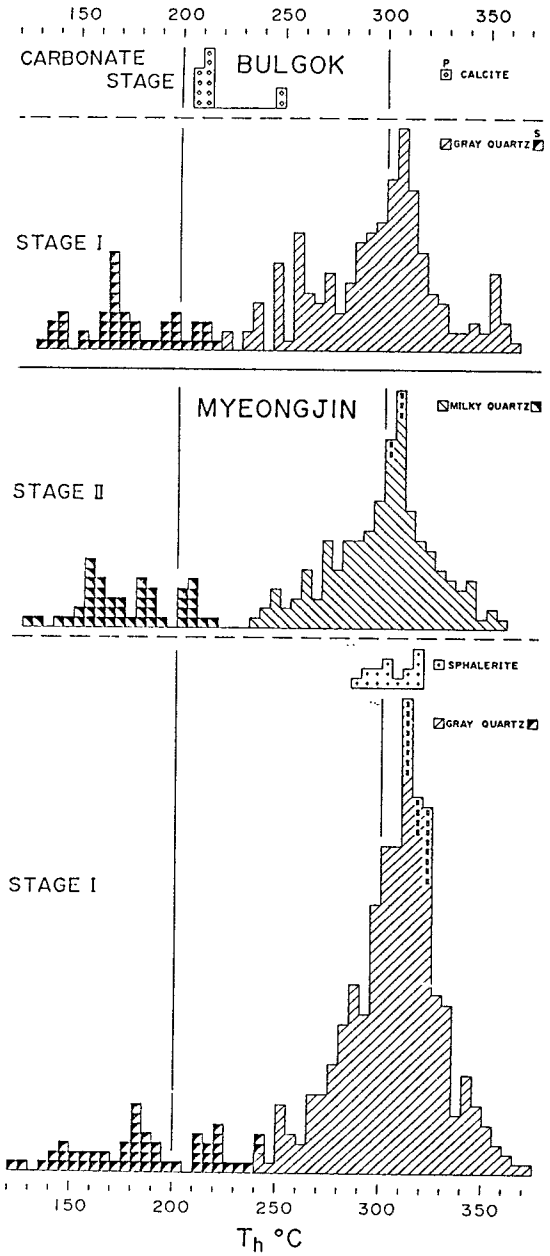

Fig. 4. Frequency diagram of homogenization temperatures of fluid inclusions in vein minerals of the Geojea Au–Ag mining area. P=primary; S= secondary; II=vapor–rich inclusions.

relationship between temperature and salinity shown in Fig. 6.

Pressure Condition

Liquid–rich type I and vapor–rich type II fluid inclusions are intimately associated in some samples of stage I and II quartz and they tend to homogenize at similar temperatures. These observations indicate that the fluids which deposited ore and gangue minerals during stage I and II periodically boiled. Therefore no pressure corrections are necessary for these inclusions because they were trapped along the two–phase boundary of the system H_2O–NaCl. The data of Sourirajan and Kennedy(1962) for the system H_2O–NaCl, combined with the temperature and salinity data for stage I and II fluids, suggest pressures of <100 bars, corresponding to maximum depths of about 500 to 1,250m, respectively, assuming lithostatic and hydrostatic loads.

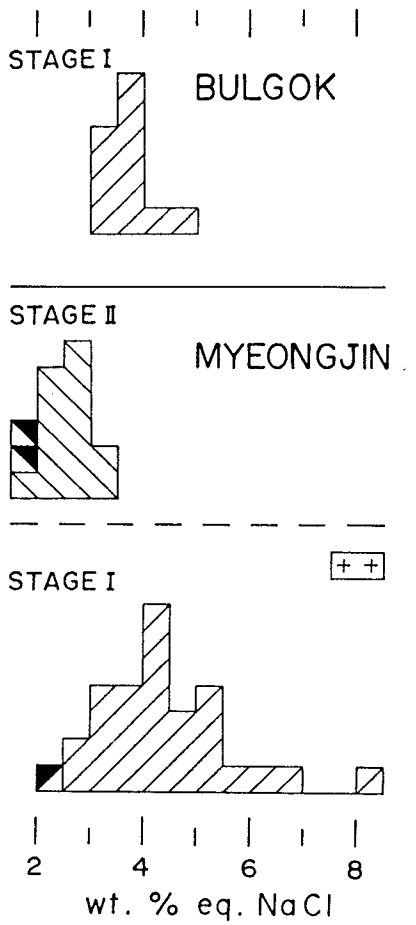

Fig. 5. Frequency diagram of salinities of fluid inclusions in vein minerals of the Geojae Au–Ag mining area. Symbols are the same as in Figure 4.

CHEMICAL ENVIRONMENT OF ORE DEPOSITION

Data obtained from the mineral assemblages,

mineral compositions and fluid inclusions have been utilized to trace the chemical evolution of the Au–Ag–bearing stage I mineralizing episode. From the paragenesis diagram in Fig. 2, it can be seen that mineral assemblages of stage I change from the early to the late substages.

Based on the homogenization temperature

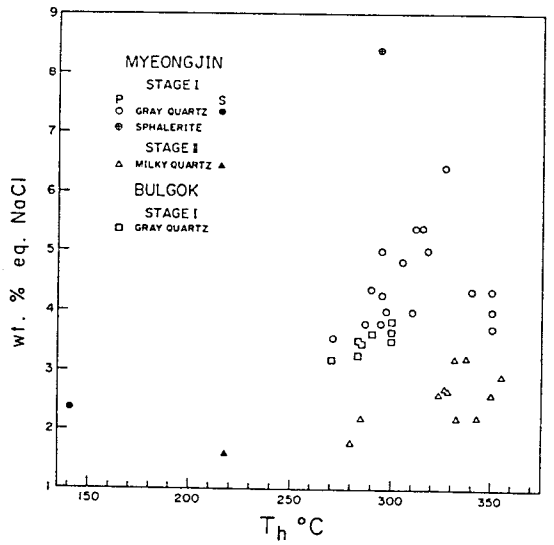

Fig. 6. Homogenization temperature versus salinity diagram for fluid inclusions in vein minerals from the Geojae Au–Ag mining area.

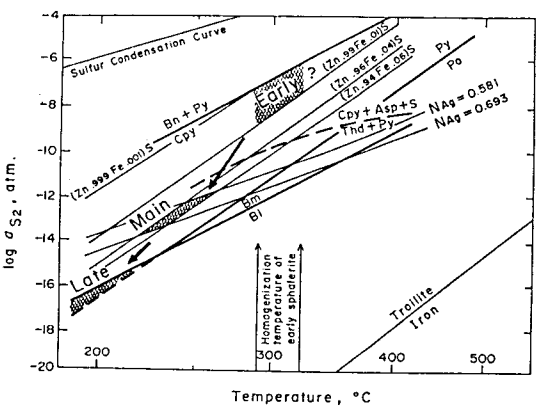

Fig. 7. Temperature–sulfur fugacity diagram showing the stability fields(hatched area) of ore minerals suggested by mineralogical assemblages observed in stage I mineralization. Reaction curves are from Barton and Skinner(1979). Asp : arsenopyrite, Bi : native bismuth, Bm : bismuthinite, Bn : bornite, Cpy : chalcopyrite, Po : pyrrhotite, Py : pyrite, Thd : tetrahedrite, N_{Ag} : atomic fraction of silver in electrum, Early : early Cu+Pb+Zn sulfide substage, Main : main Au–Ag telluride substage, Late : late Pb–Bi sulfosalts+native bismuth substage.

range of early sphalerite and quartz, and the isopleth(0.15 to 1.1 FeS mole %) of sphalerite intergrown with pyrite and chalcopyrite in the early substage, the ranges of sulfur fugacity and temperature of formation during the early ore mineralization(dominant pyrite, sphalerite and chalcopyrite) are as 10^{-6} to 10^{-10} atm. and 289 to 318℃, respectively(Fig. 7). According to the relationship between the homogenization temperature and salinity in stage I, as shown in Fig. 6, the initial ore fluids(near 370℃) boiled at about 330℃. This temperature range is similar to that of liquid–rich inclusions in early sphalerite. Boiling in hydrothermal systems can be result in abrupt chemical changes(e.g., pH, fo_2, ΣH_2S, ΣCO_2 etc.) in the liquid phase(Drummond and Ohmoto, 1985). These chemical changes may favor deposition of metals through destabilization of metal complexes (Seward, 1984 ; Cole and Drummond, 1986). Thus, boiling can be linked to early ore mineral deposition.

The FeS mole percent of sphalerite associated with electrum and stuezite in main Au–Ag telluride substage ranges from 3.85 to 5.82. The atomic fraction(N_{Ag}) of silver in electrum with stuezite in galena is between 0.58 and 0.69. Isopleths of sphalerite and electrum were estimated from Fe–Zn–S(Scott and Barnes, 1971) and Au–Ag–S(Barton and Toulmin, 1964) system. The narrow stability field for gold and silver minerals of the main substage can be set by isopleths of sphalerite and electrum in Fig. 7. The estimated sulfur fugacity and temperature of formation range from $10^{-11.8}$ to 10^{-14} atm. and 220 to 260℃, respectively. During the late mineraliza-

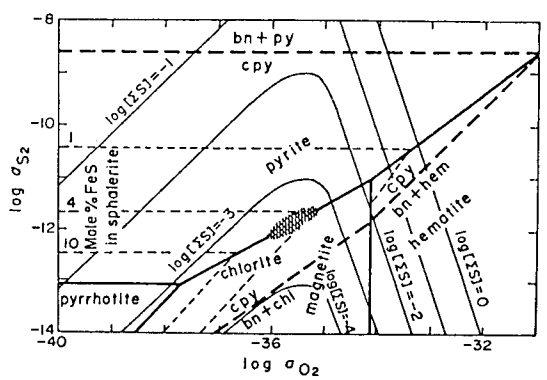

Fig. 8. Log a_{S_2}–log a_{O_2} diagram showing the total concentration of sulfur at 250℃. Hatched area is the stability field of main Au–Ag telluride depositional substage of stage I. The standard state of S_2(and O_2) is ideal diatomic gas at 1 atm and 250℃. Heavy solid lines show boundaries between pyrite, pyrrhotite, chlorite, hematite. bn : bornite, chl : chlorite, cpy : chalcopyrite, hem : hematite, py : pyrite.

tion in stage I, Pb–Bi sulfosalts and native bismuth were coprecipitated with pyrite and galena. The stability field of pyrite+native bismuth is restricted by reaction curves of pyrite–pyrrhotite and bismuthinite–native bismuth in Fig. 7. The upper limits of sulfur fugacity and temperature of the late substage are 10^{-15} atm. and 220℃, respectively.

Pyrite+chlorite+hematite enable us to estimate the chemical potentials for fs_2 and fo_2. Though iron oxides are not present, hydrothermal chlorite flakes are common inclusions both in ore minerals and in quartz in the stage I veins. Provided that we assign appropriate values of oxygen fugacity for gold–silver deposition at temperatures near 250℃, as shown in Fig. 8, pyrite+chlorite with sphalerite(3.8 to 5.8 FeS mole %) in the main substage gives an estimated oxygen fugacity range for gold–silver deposition of approximately 10^{-35} to 10^{-36} atm. The value of total concentration of sulfur is between 10^{-3} and 10^{-4} molal.

These estimated results together with a pH controlled by the potassium feldspar–sericite reaction suggest that, for a reasonable ore fluid environment, the activity of reduced H_2S is much greater than oxidized sulfur species(Fig. 9).

The linear relationship between temperature and salinity as shown in Fig. 6 indicates that later rapid cooling and dilution of ore-forming fluids by mixing with less-evolved meteoric waters led to gold–silver deposition, through the break down of metal complexes such as $Au(HS)_2^-$, as the activity of the H_2S decreased.

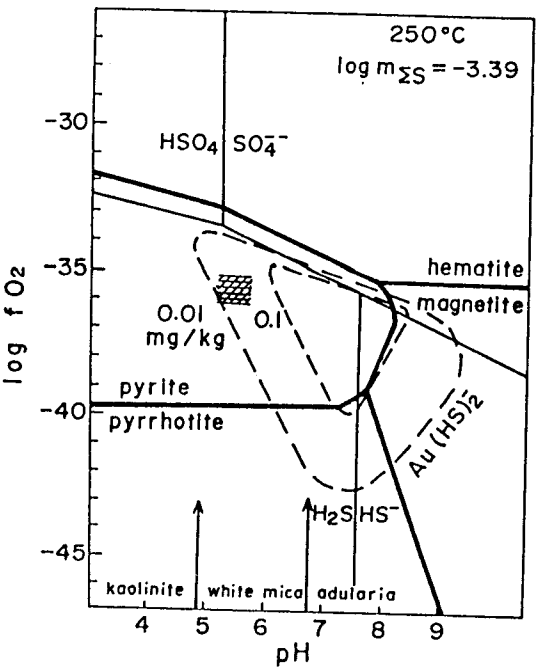

Fig. 9. Mineral and sulfur species stability diagram. The contours(dashes) show the solubility of gold in mg/kg as a bisulfide complex at 250℃ and total sulfur=$10^{-3.39}$m. Boundaries for principal sulfide species in solution(solid lines), stability fields for solid Fe sulfides and oxides-(bold lines). Hatched area is the environment of main Au–Ag telluride depositional substage of stage I.

SULFUR, CARBON AND OXYGEN ISOTOPE STUDY

Recent studies have shown the utility of stable isotopes in elucidating the origin and hydrothermal evolution of Au–Ag deposits(Taylor, 1973 ; Rye et al., 1974 ; O'Neil and Silberman, 1974 ; Casadevall and Ohmoto, 1977 ; So and Shelton, 1987 a and b, 1988 a and b, 1989 a and b). In this study we measured sulfur isotope compositions of sulfides, and oxygen and carbon isotope compositions of calcite, in order to determine the source of sulfur and carbon, and formation temperature of ore deposition in the deposit. Standard techniques of extraction and analysis were used(McCrea, 1950 ; Grinenko, 1962). Data are reported in standard natation

Table 3. Sulfur isotope data of Stage I sulfides from the Geojae Au–Ag Mining Area.

Mine	Sample no.	Mineral	$\delta^{34}S$‰	$\Delta^{34}S$‰	T℃*	$\delta^{34}S_{H_2S}$(‰)	Th℃**	coments
Myeongjin	MJI-27	sl	0.36	3.02	216°±17	−0.06	215 to 275	Main Au–Ag telluride substage
		gn	−2.66	(sl–gn)		−0.03		
	MJI-35	sl	0.29					
Bulgok	BGI-51	py	6.86	3.94	236°±20	5.3	244 to 350	Early Cu+Pb+Zn sulfide substage
		gn	2.92	(py–gn)		5.4		
	BGI-56	py	6.23					

* Isotopic equilibrium temperature

** Fluid inclusions in associated gray quartz

Abbreviations : gn=galena, py=pyrite, sl=sphalerite

Table 4. Carbon and Oxygen Isotope Data for Calcites, Geojae Au-Ag Mining Area.

Mine	Sample no.	$\delta^{13}C$(‰)	$\delta^{18}O$(‰)	T(℃)[1]	$\delta^{13}C_{CO_2}$(‰)[2]	$\delta^{18}O_{water}$(‰)[3]
Myeongjin	MJ-2	-8.7	6.4	210	-8.1	2.0
Bulgok	BG-1	-5.4	11.0	210	-4.8	-2.6

1) ; Based on fluid inclusion temperatures.
2) ; Calculated CO_2 carbon isotope compositions based on calcite-CO_2 carbon isotope fractionation equation of Friedman and O'Neil(1977).
3) ; Calculated water composition based on calcite-water oxygen isotope fractionation equation of Friedman and O'Neil(1977).

relative to the CDT for S, the PDB for C, and the Vienna SMOW for O. The analytical error is approximately ±0.1‰ for S, C, and O.

Sulfur isotope analyses were performed on 6 hand-picked stage I sulfides from the Bulgok and Myeongjin mines(Table 3). Pyrites and galena occurring in early Cu+Pb+Zn sulfide substage from the Bulgok mine have $\delta^{34}S$ values of 6.23 to 6.86‰ and 2.92‰, respectively. Sphalerite and galena in main Au-Ag telluride substage from the Myeongjin mine have $\delta^{34}S$ values of 0.23 to 0.36‰ and -2.66‰, respectively. Pyrite-galena and sphalerite-galena pairs with equilibrium textures have $\Delta^{34}S$ values of 3.94‰ and 3.02‰, respectively, yielding 236±20℃ and 216±17℃(Ohmoto and Rye, 1979). These temperatures are in agreement with homogenization temperatures in primary inclusions in the associated gray quartz. Based on isotopic equilibrium temperatures, the calculated $\delta^{34}S$ values for H_2S during early Cu+Pb+Zn sulfide substage and main Au-Ag telluride substage are near 5.3 to 5.4‰ and -0.03 to -0.06‰, respectively. Because of the small isotopic fractionation between aqueous H_2S and sulfides, the isotopic composition of the total sulfur in the hydrothermal system($\delta^{34}S_{\Sigma S}$) is near 0 to 5‰. The $\delta^{34}S$ is near the meteoric standard and comparable to sulfur of known mantle origin.

The isotopic composition of S in igneous rocks derived from the mantle is similar to that of meteorites(Shima et al., 1963 ; Smitheringale and Jensen, 1963). Schneider(1970) reported an average $\delta^{34}S$ value of 1.3±0.5‰ for alkali olivine basalts. Kanehiro(1973) obtained $\delta^{34}S$ values ranging from 0.3 to 1.6‰ for tholeiites from the Mid-Atlantic Ridge at 30°N. However, sulfide minerals in granitic rocks have more variables ranging from 9 to -4‰ for European granites(Hoefs, 1980), and from 9 to -11‰ for granitic rocks in Japan(Sasaki and Ishihara, 1979). Coleman(1979) has pointed out that the isotope composition of S in granite may depend on the fo_2 of the magma. Ohmoto and Rye(1979) have shown that a magmatic fluid phase in equilibrium with a hydrous granitic melt(log fo_2=-12, 1000 bars, 800℃, initial $\delta^{34}S$ melt value near 0‰) will have a $\delta^{34}S$ fluid value near 4‰. We therefore interpret the source of sulfur in the Geojae Au-Ag deposits an igneous source, possibly the nearby Cretaceous granite.

Analyses of carbon and oxygen isotopes were performed on two carbonate stage calcites from the Myeongjin and Bulgok mines. The $\delta^{13}C$ values are -8.7‰ for the Myeongjin and -5.4‰ for the Bulgok(Table 4). Using the calcite-CO_2 carbon isotope fractionation equation of Friedman and O'Neil(1977), coupled with fluid inclusion temperatures, the calculated $\delta^{13}C_{(CO_2}$ values are -8.1 and -4.8‰, respectively. These carbon isotope data may be compatible with a deep igneous carbon source(Burrows and Spooner, 1987).

The $\delta^{18}O$ values of the calcites are 6.4 and 11.0‰(Table 4). Calculated $\delta^{18}O$ water values are -2.6 and 2.0‰, using the calcite-water isotope fractionation equation of Friedman and O'Neil(1977). Coupled with the previous hydrogen isotope data for the Korean Cretaceous epithermal Au-Ag deposits(Shelton et al., 1988 ; So et al., 1989), the calculated $\delta^{18}O$ water values for the calcites possibly indicate a dominance of meteoric water component, approaching unexchanged paleometeoric water values.

REFERENCES

Barton, P. B., Jr., and Skinner, B. J., 1979, Sulfide mineral stabilities, In geochemistry of hydrothermal ore deposits(Barnes, H. L. Ed.), p. 798. Wiley and Sons Pub. Co., New York, p. 278-403.

Barton, P. B. Jr., P. Toulmin, III, 1964, The electrum-tranish method for the determination of the fugacity of sulfur in labratory sulfides system

: Geochim. Cosmochim. Acta., v. 28, p. 619–640.

Burrow, D. R., and Spooner, E. T. C., 1987, Generation of a magmatic H_2O–CO_2 fluid enriched in Mo, Au, and W within an Archean sodic granodiorite stock, Mink Lake, north western Ontario : Econ. Geol., v. 82, p. 1931–1957.

Cole, D. R., and Drummond, S. E., 1986, The effect of transport and boiling on Ag/Au ratios in hydrothermal solutions : A preliminary assessment and possible implications for the formation of epithermal precious-metal ore deposits : Jour. Geochem. Explor., v. 25, p. 45–79.

Coleman, M. L., 1979, Isotopic analyses of trace sulfur from some S-and I-type granites : Heredity or environment ? In M.P. Atherton and J. Tarney, eds. Origin of Granite Batholiths Geochemical Evidence, p. 129–133. Shiva Publ. Co.

Drummond, S. E., 1981, Boiling and mixing of hydrothermal fluids : chemical effects on mineral precipitation : Unpub. Ph. D. thesis, Pennsylvania State Univ., 380 p.

Drummond, S. E., and Ohmoto, H., 1985, Chemical evolution and mineral deposition in boiling hydrothermal systems : Econ. Geol., v. 80, p. 126–147.

Friedman, I., and O'Neil, J. R., 1977, Compilation of stable isotope fractionation factors of geochemical interest. in Fleisher, M., ed., Data of geochemistry, Sixth Edition : U.S. Geol. Survey Prof. Paper 440-KK, P. KK1–KK12.

Grinenko, V. A., 1962, Preparation of sulfur dioxide for isotopic analysis : Zeitschr. Neorgan. Khimii, v. 7, p. 2478–2483.

Kanehiro, K., Yui, S., Sakai, H., and Sasaki, A., 1973, Sulphide globules and sulphur isotope ratios in the abyssal tholeiite from the Mid-Atlantic Ridge near 30°N latitude. Geochem. Journal, v. 7, p. 89–96.

Ohmoto, H., 1972, Systematics of sulfur and carbon isotopes in hydrothermal ore deposits : Econ. Geol., v. 67, p. 551–578.

Park, H. I., 1983, Ore and fluid inclusions of the Tongyeong gold-silver deposits : Jour. Korean Inst. Mining Geology, v. 16, p. 245–251(in Korean).

Potter, R. W. III, Clynne, M. A., and Brown, D. L., 1978, Freezing point depression of aqueceous sodium chloride solutions : Econ. Geol., v. 73, p. 284–285.

Poty, B., Leroy, J., and Jachimowicz, L., 1976, Un nouvel appareil pourla mesure des temperatures, sous le microscope : l'Installation de micro-thermometrie Chaizmeca : Soc. francaise Mineralogie Cristallographie Bull., v. 99, p. 182–186.

Sasaki, A., and Ishihara, S., 1979, Sulfur isotopic composition of the magnetite-series and ilmenite-series graintoids in Japan. Contrib. Mineral. and Petrol., v. 68, p. 107–115.

Schneider, A., 1970, The sulfur isotope composition of basaltic rocks. Contrib. Mineral. Petrol., v. 25, p. 95–124.

Scott, S. D. and H. L. Barnes, 1971, Sphalerite geothermometry and geobarometry · Econ. Geol., v. 66, p. 653–669.

Seward, T. M., 1984, The transport and deposition of gold in hydrothermal system. In gold '82 : The geology, geochemistry and genesis of gold deposits(Hoste. R. p., ed.) Rotterdam : ema 753p., 165–181.

Shikazono, N., 1985, A comparision of temperatures estimated from the electrum sphalerite-pyrite-argentite assemblage and filling temperatures of fluid inclusions from epithermal Au-Ag vein type deposits in Japan : Econ. Geol., v. 80, p. 1415–1424.

Shikazono, N. and Shimizu, M., 1986, Compositional variations in Au-Ag series mineral from some gold deposits in Korean peninsula : Mining Geology, v. 36, p. 545–553.

Shima, M., Gross, W. H. and Thode, H. G., 1963, Sulfur isotope abundances in basic sills, differentiated granites, and meteorites. J. Geophys., Res., 68, No. 9. 2835–2847.

Shimazaki, H., Sato, K., and Chon, H. T., 1981, Mineralization associated with Mesozoic felsic magmatism in Japan and Korea : Mining Geology, v. 31, p. 297–310.

Shimazaki, H., Lee, M. S., Tsusue, A., and Kaneda, H., 1986, Three epoch of gold mineralization in South Korea : Mining Geology, v. 36, p. 265–272.

Shelton, K. L., So, C. S., and Chang, J. S., 1988, Gold-rich mesothermal vein deposits of the Republic of Korea : Geochemical studies of the Jungwon gold area : Econ, Geol., v. 83, p. 1221–1237.

Smitheringale, W. G., and Jensen, M. L., 1963, Sulfur isotopic composition of the Triassic igneous rocks of eastern United States. Geochim. Cosmochim. Acta, 27, p. 1183–1207.

So, C. S., Chi, S. J., and Shelton, K. L., 1988, Stable isotope and fluid inclusion studies on gold-silver-bearing vein deposits, Cheonnan--Cheongyang-Nonsan mining district, Republic of Korea : Nonsan area : Neues Jahrbuch Miner. Abh., v. 158, p. 47–65.

So, C. S., Chi, S. J., Yu, J. S., and Shelton, K. L., 1987a, The Jeonui gold-silver mine, Republic of Korea : A geochemical study : Mining Geology, v. 37, p. 313–322.

So, C. S., Choi, S. H., and Chi, S. J., 1987b, Genetic environments of the Geumryong gold--silver deposit, Korea : Jour. Geol. Soc. Korea, v. 23, p. 321–330.

So, C. S., and Shelton, K. L., 1987a, Stable isotope and fluid inclusion studies of gold-silver--bearing hydrothemal vein deposits, Cheonan--Cheongyang-Nonsan mining district, Republic of Korea : Cheonan area : Econ. Geol., v. 82, p. 987–1000.

So, C. S., and Shelton, K. L., 1987b, Fluid inclusion and stable isotope studies of gold- silver bearing hydrothermal vein deposits, Yeoju mining district, Republic of Korea : Econ. Geol., v. 82, p. 1309–1318.

So, C. S., Yun, S. T., and Chi, S. J., 1989, Geochemical studies of hydrothermal gold-silver deposits, Republic of Korea : Yangdong mining district : Jour. Geol. Soc. Korea, v. 1, p. 16–29.

Sourirajan, S. and Kennedy, G. C., 1962, The system H_2O-NaCl at elevated temperatures and prssures : Amer. Jour. Sci., v. 260, p. 115-141.
Sugaki, A., Kim, O. J., and Kim, W. J., 1986, Gold and silver ores from the Geumwang mine in South Korea and their mineralization : Mining Geology, v. 36, p. 555-572.
Tsuchida, T., 1944, Ore deposits in Korea, Kasumigaseki Book Co., Tokyo 329p.(in Japanese).
Tsusue, A., Mizuta, T., Watanabe, M. and Min, K. G., 1981, Jurassic and Cretaceous granitic rocks in South Korea : Mining Geology, v. 31, p. 1261-1280.
Won, C. K., Chi, J. M., Kim, S. J., Yoon, S., So, C. S., and Kim, H. S., 1980, Geologic sheet of Geoje and Yulpo area : Korea Geol. Survey, 1 : 50,000.

巨濟지역 金-銀광상의 鑛化作用 연구

崔善奎 · 池世定 · 尹聖澤 · 高龍權 · 劉宰臣

요약: 경남 거제지역 金-銀鑛床들은 후기 백악기 안산암류와 화강섬록암(83 m.y.)내의 열극을 충진한 含金-銀 熱水脈狀 광체로 구성된다. 熱水鑛化作用은 구조운동에 의하여 시기적으로 3회에 걸쳐 진행되었다. 초기 제 370℃의 고온에서 후기 200℃에 이르는 제 I, II 鑛化期에서는 각기 상이한 熱水系에 의하여 석영, 유화물이 침전하였으며, 320℃를 전후로 하여 鑛化流體의 沸騰현상이 일어났다. 제 I, II 鑛化作用시의 압력은 <100기압이고, 심도는 500~1,250m였다.

金-銀의 主鑛化時期인 鑛化 I 期의 공생광물에 대한 流體包有物 및 鑛物熱水學的 연구에 의하면, 황철석, 섬아연석, 황동석은 290℃ 이상의 고온에서 沸騰作用과 동시에 정출하였고, 사면동석, 에렉트럼, 스튜자이트는 金-硫黃種의 농도가 10^{-3}~10^{-4}molal, 相當鹽濃度가 2~6wt.% NaCl인 鑛化流體로부터 220~260℃, 유황 및 산소분압이 각각 $10^{-11.8}$~10^{-14}, 10^{-35}~10^{-36}atm인 물리 · 화학적 환경하에서 침전하였다. 均質化 온도와 鹽濃度와의 관계는 天水流入에 의한 鑛化流體의 冷却 및 稀釋작용이 광석광물 침전의 주된 메키니즘이었음을 지시해 주며, 流體內 還元 硫黃種(H_2S)의 감소에 따른 金硫化複合體($Au(HS)^-_2$)의 파괴로 金의 침전이 유도되었으리라 사료된다. 유황 및 탄소, 산소 安定同位元素 硏究결과, 鑛化流體內의 유황 및 탄소는 深部火成기원이었고, 방해석의 산소 安定同位元素값으로부터 熱水系에서 天水가 지배적인 역할을 하였으리라 사료된다.